Hydraulics of the Developing Flow Region of Stepped Spillways. I: Physical Modeling and Boundary Layer Development

Gangfu Zhang[1] and Hubert Chanson[2]

Abstract: On a stepped spillway, the steps act as macroroughness elements, contributing to enhanced energy dissipation and significant aeration. In a skimming flow, the upstream flow motion is nonaerated, and the free surface appears smooth and glossy up to the inception point of free-surface aeration. In this developing flow region, a turbulent boundary layer grows until the outer edge of the boundary layer interacts with the free surface and air entrainment takes place. The flow properties in the developing flow region were documented carefully in a large stepped spillway model (1V:1H; $h = 0.10$ m). The upstream flow was controlled by a broad-crested weir and critical flow conditions were observed along most of the weir crest, although the pressure distributions were not hydrostatic at the upstream and downstream ends. Downstream of the broad crest and upstream of the inception point, the free surface was smooth, although some significant free-surface curvature was observed for all discharges. The boundary layer growth was faster than on a smooth chute for identical flow conditions. The inception point of free-surface aeration was observed when the boundary layer thickness reached 80% of the flow depth: $\delta/d_i \approx 0.8$. The location of the inception point of free-surface aeration and the flow depth at inception were compared successfully to previous laboratory and prototype results. **DOI: 10.1061/(ASCE)HY.1943-7900.0001138.**

Author keywords: Stepped spillways; Developing flow region; Physical modeling; Boundary layer development; Inception point of air entrainment.

Introduction

Historical records indicate that stepped spillways have been used for thousands of years (Chanson 1995, 2000–2001). The steps act as macroroughness elements, contributing to enhanced energy dissipation and significant aeration. With most typical design flow conditions, the water skims down the stepped chute as a large coherent stream—i.e., in a skimming flow regime (Rajaratnam 1990; Peyras et al. 1992) (Fig. 1). Upstream of the chute, the free surface is smooth and glassy, with a developing boundary layer underneath. When the boundary layer outer edge starts to interact with the free surface, the turbulent shear stresses overcome the combined buoyancy and surface tension and initiate a process of rapid air entrainment (Fig. 1). Fig. 1 presents a prototype stepped spillway operation; the location of the inception point is clearly marked. For high specific discharges, the boundary layer may not reach the surface, and aeration may not occur along a stepped chute. This situation is particularly relevant to small to medium-sized dams operating with large unit discharges (Gonzalez and Chanson 2007; Meireles and Matos 2009). In the absence of self-aeration, the spillway might be prone to cavitation damage, although all the prototype observations indicated an absence of cavitation pitting and damage to the steps (Chanson 2001, 2015; Frizell et al. 2013).

For the last two decades, a majority of the research on stepped chutes has focused on the hydraulics of the self-aerated flow region downstream of the inception point. The developing flow region was less studied. Amador et al. (2006, 2009), Hunt and Kadavy (2010), and Meireles et al. (2012) investigated the clear-water flow depth, boundary layer growth, and velocity profiles, while Meireles et al. (2014) tested several air entrainment onset criteria. The time-averaged velocity, boundary layer development, and water-level data were reproduced successfully using computational fluid dynamics modeling (Bombardelli et al. 2011) for a limited set of experimental data.

The present study aims to provide a new characterization of the developing flow region on a stepped spillway. Experiments were performed in a large, steep-stepped chute (1V:1H) to characterize the free-surface profile and boundary layer development. The flow properties in the developing boundary layer and at the inception point of free-surface aeration are discussed in this paper. In a companion paper, the velocity and pressure fields are discussed (see Part II; Zhang and Chanson 2016).

Physical Modeling, Experimental Facility, and Instrumentation

Presentation

Hydraulic models are commonly used during the design stage to optimize a stepped spillway. In a physical model, the flow conditions must be similar to those at full sale. Considering the developing flow region on a rectangular prismatic stepped channel, a simplified dimensional analysis leads to a number of relationships

[1]Ph.D. Research Student, School of Civil Engineering, Univ. of Queensland, Brisbane, QLD 4072, Australia.

[2]Professor, Dept. of Hydraulic Engineering, School of Civil Engineering, Univ. of Queensland, Brisbane, QLD 4072, Australia (corresponding author). E-mail: h.chanson@uq.edu.au

Note. This manuscript was submitted on May 28, 2015; approved on December 21, 2015; published online on March 22, 2016. Discussion period open until August 22, 2016; separate discussions must be submitted for individual papers. This paper is part of the ***Journal of Hydraulic Engineering***, © ASCE, ISSN 0733-9429.

Fig. 1. Paradise dam (Australia) stepped spillway operation on March 5, 2013 (shutter speed: 1/1,600 s)—$d_c/h = 2.85$, $\mathsf{R} = 2.9 \times 10^7$, $h = 0.62$ m—the arrow points to the inception point of free-surface aeration

between the clear-water flow properties, fluid properties, and boundary conditions:

$$\frac{d}{d_c}, \frac{V_x}{V_c}, \frac{P}{\rho \times g \times d_c}, \ldots = F_1\left(\frac{x}{d_c}, \frac{y}{d_c}, \frac{z}{d_c}, \frac{d_c}{h}, \rho \times \frac{U \times D_H}{\mu}, \frac{g \times \mu^4}{\rho \times \sigma^3}, \frac{W}{d_c}, \theta, \ldots.\right) \quad (1)$$

where d = water depth measured perpendicular to the pseudo-bottom formed by the step edges; V_x = longitudinal velocity component; P = pressure; d_c and V_c = critical flow depth and velocity, respectively; x, y, and z = longitudinal, normal, and transverse coordinates, respectively; U = depth-averaged velocity; D_H = hydraulic diameter; W = channel width; h = vertical step height; g = gravity acceleration; θ = chute slope; μ = dynamic viscosity of water; ρ = water density; and σ = surface tension between air and water. In Eq. (1), the dimensionless clear-water flow properties at a location (x, y, and z) are expressed as functions of dimensionless parameters, including the dimensionless discharge d_c/h, Reynolds R, and Morton M numbers. Note that the dimensionless discharge d_c/h is proportional to a Froude number defined in terms of the step height since $d_c/h = (q/\sqrt{g \times h^3})^{2/3}$ where q is the water discharge per unit width.

In the present study, Froude and Morton similarities were used, the chute slope ($\tan\theta = h/l$) and the channel width W were kept constant, and the measurements were conducted on the channel centerline. Thus, Eq. (1) became

$$\frac{d}{d_c}, \frac{V_x}{V_c}, \frac{P}{\rho \times g \times d_c}, \ldots = F_2\left(\frac{x}{d_c}, \frac{y}{d_c}, \frac{d_c}{h}, \rho \times \frac{U \times D_H}{\mu}, \ldots.\right) \quad (2)$$

The present experiments were conducted in a large facility that operated with large Reynolds numbers (Table 1). These conditions corresponded to a 1:6-scale study of a typical prototype stepped spillway, such that shown in Fig. 1 (neglecting the effects of chute slope and inflow conditions), ensuring that the extrapolation of the laboratory data to prototype conditions is unlikely to be adversely affected by scale effects.

Table 1. Laboratory Studies of the Developing Flow Region on Stepped Spillways

Reference	θ (°)	h (m)	W (m)	Crest design	q (m^2/s)	d_c/h	Instrumentation	Remarks
Present study	45.0	0.10	1.0	Broad crest with u/s and d/s rounding	0.085–0.216	0.9–1.7	Prandtl-Pitot tube ($\emptyset = 3.18$ mm), double-tip conductivity probe ($\emptyset = 0.25$ mm)	AEB hydraulics laboratory (UQ)
Amador et al. (2006)	51.3	0.05	0.5	WES ogee with 3 small steps	0.11	2.15	Particle image velocimetry (PIV)	Experiments in setup #2 (UDC) by Amador (2005)
Meireles et al. (2012)	53.1	0.08	1.0	WES ogee with small steps	0.08–0.20	1.1–2.0	Back-flushing Pitot tube, conductivity probe	Experiments at LNEC by Matos (1999)
		0.04	1.0	WES ogee with small steps	0.05–0.18	1.6–3.7	Back-flushing Pitot tube, conductivity probe	Experiments at LNEC by Meireles (2004)
		0.04	1.0	WES ogee with	0.10 and 0.20	2.5 and 4.0	Back-flushing Pitot tube,	Experiments at LNEC
		0.02	1.0	small steps	0.10–0.20	5.0–8.0	conductivity probe	by Renna (2004)

Note: d_c = critical flow depth; h = vertical step height; q = water discharge per unit width; W = channel width; θ = slope angle with horizontal.

Fig. 2. Experimental facility and spillway model operation for $q = 0.22$ m^2/s, $d_c/h = 1.7$, $\mathrm{R} = 8.7 \times 10^5$—the arrow points to the inception point of free-surface aeration

Experimental Flume and Instrumentation

Experiments were performed in a new, large stepped spillway model (1V:1H) at the University of Queensland (Fig. 2). The flow was delivered by three pumps driven by adjustable frequency alternating current (AC) motors. Water was fed into a 1.7-m-deep, 5-m-wide intake basin with a surface area of 2.7×5 m^2, leading to a 2.8-m-long sidewall convergent with a contraction ratio of 5.08:1, resulting in a smooth and waveless flow in the 0.985-m-wide test section. The inflow upstream of the test section was controlled by a broad-crested weir. The weir consisted of a 1.2-m-high, 0.60-m-long, and 0.985-m-wide crest with a vertical upstream wall, an upstream rounded nose (with a 0.058-m radius), and a downstream rounded edge (with a 0.012-m radius). The test section was equipped with 12 impervious flat steps (Fig. 2), each of which was 0.1 m long, 0.1 m high, and 0.985 m wide.

Clear-water flow depths were measured with a pointer-gauge on the channel centerline. The free-surface profiles were photographed and water-level data were checked with a dual-tip phase detection probe on the steep chute, sampled at 20 kHz per sensor for 45 s. The accuracy of the pointer gauges was ± 1 mm in the clear-water flow region. Total and static head measurements were performed above the broad crest and on the stepped chute in the clear-water flow region with a Dwyer 166 Series Prandtl-Pitot tube ($Ø = 3.18$ mm). The tube featured a hemispherical total pressure tapping ($Ø = 1.19$ mm) and four equally spaced static pressure tappings ($Ø = 0.51$ mm) located 25.4 mm behind the tip. The tip design met Air Movement and Control Association (AMCA) and American Society of Heating and Air-Conditioning Engineers (ASHRAE) specifications. Any effect resulting from the longitudinal separation between the total and static tappings was taken into account by repeating the independent total and piezometric head measurements at each location. The Prandtl-Pitot tube was connected to an inclined manometer, with the tubes opened to the atmosphere to give total head and piezometric head readings. The error on the Prandtl-Pitot tube reading was less than 1 mm vertically. The vertical movement of the probe was controlled by a fine adjustment traveling mechanism connected to a Mitutoyo digital scale, giving an accuracy of less than ± 0.1 mm in the direction normal to the inversion. The accuracies of the longitudinal and transverse positions of the tube were estimated to be ± 0.5 cm and ± 1 mm, respectively. Additional observations were recorded with digital single lens reflex (dSLR) cameras. Further details were reported in Zhang and Chanson (2015).

Experimental Flow Conditions

Although the present study focused on the skimming flow regime, preliminary tests showed that a nappe occurred for $d_c/h < 0.4$. A transition flow was observed for $0.4 < d_c/h < 0.9$, and skimming flows were seen for $d_c/h > 0.9$. The changes in flow regimes were consistent with the literature (Chanson 2001; Chanson and Toombes 2004).

Herein, the developing flow measurements focused on the skimming flow regime ($d_c/h > 0.9$). The experimental flow conditions are summarized in Table 1 and compared to previous detailed experimental investigations.

Spillway Crest Operation

The discharge on the steep-stepped chute was controlled by the upstream broad-crested weir (Fig. 2). Visual observations and Prandtl-Pitot tube measurements were conducted to characterize the flow conditions above the weir crest. Quiescent inflow conditions were observed for all investigated discharges above the broad-crested weir. The flow accelerated above the upstream rounded nose. Next to the upstream end of the crest, the flow was rapidly varied and characterized by some rapid changes in free-surface curvature and pressure and velocity distributions. For moderate-sized to large discharges ($H_1/L_{\mathrm{crest}} > 0.17$), the free surface fell continuously in the flow direction [Fig. 3(a)], where H_1 is the upstream total head above crest and L_{crest} is the crest length ($L_{\mathrm{crest}} = 0.60$ m). For the smallest discharges ($H_1/L_{\mathrm{crest}} < 0.11$), the water surface above the crest showed a characteristic wavy shape and the overflow was subcritical over most of the crest length. This characteristic was most likely the consequence of the effect of a developing boundary layer at low flow rates (Isaacs 1981; Chanson 1996).

The discharge was deduced from detailed velocity and pressure measurements performed above the broad-crested weir, which gave

$$q = \left(0.8966 + 0.243 \times \frac{H_1}{L_{\mathrm{crest}}}\right) \times \sqrt{g \times \left(\frac{2}{3} \times H_1\right)^3} \quad (3)$$

Above the crest, the depth-averaged specific energy may be expressed as (Liggett 1993; Chanson 2006)

$$E = \frac{\int_0^d \{[V_x^2/(2 \times g)] + y + [P/(\rho \times g)]\} \times dy}{d} = \beta \times \frac{U^2}{2 \times g} + \Lambda \times d \quad (4)$$

where E = depth-averaged specific energy, y = distance normal to the invert, U = depth-averaged velocity, β = Boussinesq coefficient (i.e., momentum correction coefficient), and Λ = pressure coefficient, defined as

$$\Lambda = \frac{1}{2} + \frac{1}{d} \times \int_0^d \frac{P}{\rho \times g \times d} \times dy \quad (5)$$

Assuming a uniform velocity profile ($\beta = 1$) and a hydrostatic pressure distribution ($\Lambda = 1$), Eq. (5) reduces to the classical expression: $E = d + 0.5 \times U^2/g$. In an open channel, critical flow conditions occur when the specific energy is minimal: $E = E_{\mathrm{min}}$ (Bakhmeteff 1932; Henderson 1966). For a smooth crest overflow, a unique relationship was proposed between the critical depth d_c,

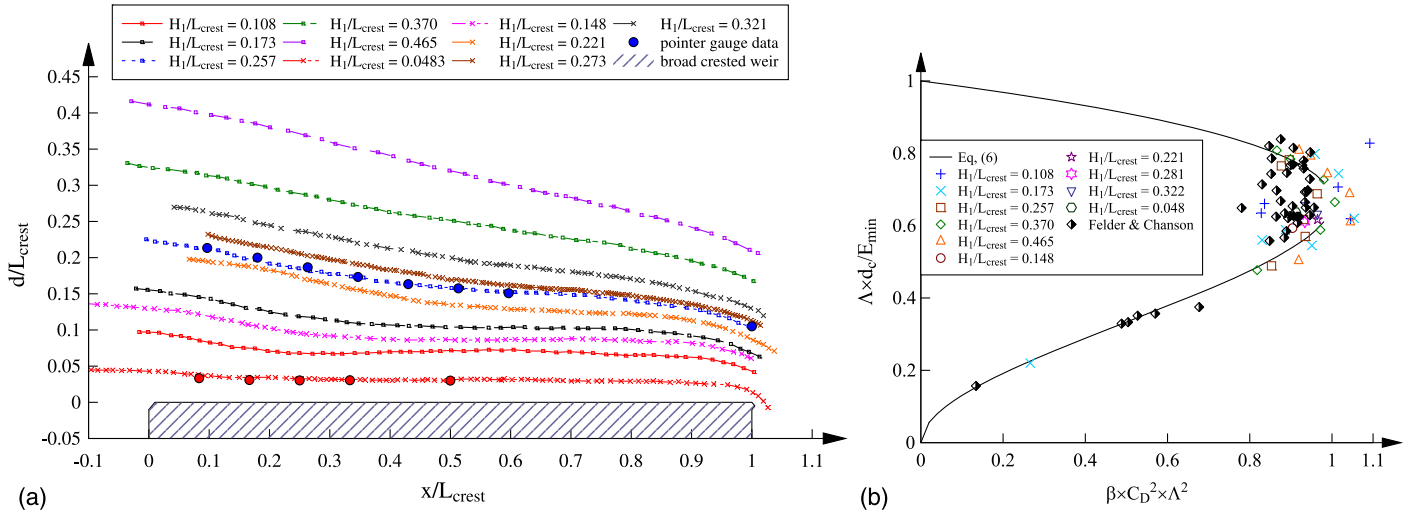

Fig. 3. Broad-crested weir operation: (a) dimensionless free-surface profiles—photographic and pointer gauge (solid circles) data; (b) dimensionless critical flow depth as a function of the discharge coefficient—comparison between rounded broad-crested weir data (data from Felder and Chanson 2012) (L_{crest} = 1.01 m; current study) and theoretical solutions (data from Chanson 2006)

the minimum specific energy E_{min}, the dimensionless discharge coefficient C_D, and the pressure and momentum coefficients Λ and β (Chanson 2006):

$$\left(\frac{d_c}{E_{min}}\right)^3 - \left(\frac{d_c}{E_{min}}\right)^2 \times \frac{1}{\Lambda} + \frac{1}{2} \times \frac{\beta \times C_D^2}{\Lambda} \times \left(\frac{2}{3}\right)^3 = 0 \qquad (6)$$

The solutions in terms of the dimensionless critical depth $d_c \times \Lambda/E_{min}$ are plotted in Fig. 3(b), where the theoretical result are compared with experimental data on broad-crested weirs (Felder and Chanson 2012, and the current study). For $0.17 < x/L_{crest} < 0.83$, a reasonable agreement was obtained between the present data and theoretical solutions. The findings suggested that critical flow conditions occurred along most of the crest length (i.e., $0.17 < x/L_{crest} < 0.83$), and this was consistent with the findings of Felder and Chanson (2012).

Flow Patterns on Stepped Spillway Chute

The present investigation focused on the skimming flow regime, which is typical of most design flow conditions for modern gravity dam-stepped spillways. For $d_c/h > 0.9$, the flow skimmed over the pseudobottom formed by the step edges and the streamlines were approximately parallel. At the upstream end, the free surface appeared glossy (Fig. 2). Some free-surface undulation was observed approximately in phase with the steps for all skimming discharges. Farther downstream, the free surface fluctuated significantly as the boundary layer developed. When the outer edge of the developing boundary layer reached the vicinity of the free surface, the turbulent shear stresses acting next to the free surface dominated over the combined effects of surface tension and buoyancy, causing air entrainment (Rao and Rajaratnam 1961; Ervine and Falvey 1987; Chanson 2008). The instantaneous location of the inception point of free-surface aeration (as discussed later in this paper) was influenced by the boundary layer fluctuations. Below the pseudobottom, the cavity fluid exhibited a circulatory motion sustained by external momentum transfer from the mainstream flow. A close examination of the cavity vortices revealed irregular ejections of fluid from the cavity into the mainstream next to the upper portion of the vertical step face, and replacements of cavity fluid next to the step edge. These observations indicated a high degree of mainstream-cavity interactions, as discussed by Rajaratnam (1990), Chanson et al. (2002), and Guenther et al. (2013). Downstream of the inception point of free-surface aeration, the flow was self-aerated, and air-water-flow measurements showed that the velocity profiles were fully-developed.

Typical dimensionless free-surface profiles are plotted in Fig. 4(a) in terms of the normalized streamwise distance L/L_i, where L is the distance from the weir's downstream end, measured along the pseudobottom, and L_i is the inception point location. For the largest discharge ($d_c/h = 1.7$), the data were checked against the equivalent clear-water depth derived from phase-detection probe measurements:

$$d = \int_0^{Y_{90}} (1 - C) \times dy \qquad (7)$$

where C = void fraction; and Y_{90} = characteristic elevation, where $C = 0.90$. These data are represented in Fig. 4(a) with red star symbols. The results showed close agreement between the pointer gauge and phase-detection probe data [Fig. 4(a)]. Some slight differences were observed downstream close to the inception point and might be on account of rapid free-surface flapping induced by turbulence, as observed in earlier studies (Chamani 2000; Chanson 2001). The free-surface profiles revealed a wavy free surface for all discharges [Fig. 4(a)]. The wavelength of the surface waves was about two step-cavity lengths, and the surface wave amplitude was the largest above the first few steps and gradually decreased in the flow direction for a given discharge. The free-surface curvature was significant for the smaller discharges, with an estimated radius of curvature as small as 0.2 m (i.e., r/h as low as 2). Since the free surface was the upper streamline, the streamline curvature implied some vertical acceleration in the upper flow column and nonhydrostatic pressure distributions (see Part II, Zhang and Chanson 2016).

Boundary Layer Development

At the upstream end of the stepped chute, a turbulent boundary layer developed along the stepped invert up to the inception point

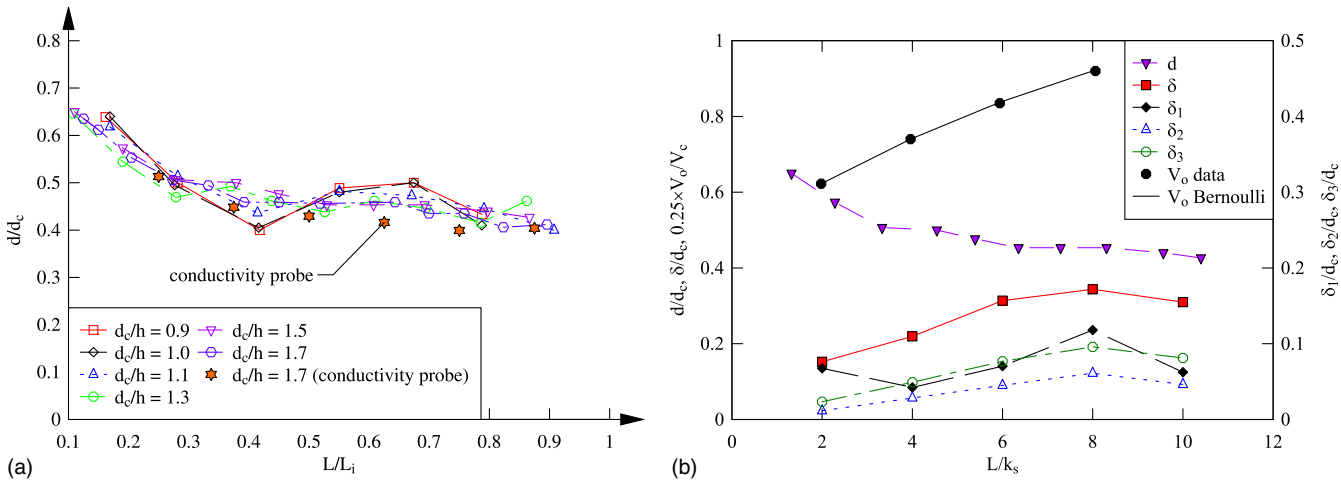

Fig. 4. Free-surface profiles and boundary layer growth in the developing flow region above the stepped chute: (a) longitudinal profiles of dimensionless water depth upstream of the inception point of free-surface aeration; (b) longitudinal profile of boundary layer thickness, displacement thickness, momentum thickness, and energy thickness data—comparison with the observed water depth and free-stream velocity-flow conditions: $d_c/h = 1.5$, $h = 0.10$ m; note the different scales of the left and right vertical axes

where the boundary layer outer edge interacted with the free surface (Wood et al. 1983; Chanson 1994). Upstream of the inception point of aeration, the water column consisted of a turbulent boundary layer and an ideal flow region above it. The basic characteristics of the developing boundary layer were derived from the measured velocity profiles (see Part II, Zhang and Chanson 2016). These were the boundary layer thickness δ, displacement thickness δ_1, momentum thickness δ_2, and energy thickness δ_3. Note that the boundary thickness was herein defined in terms of 99% of the free-stream velocity V_o. Fig. 4(b) presents typical longitudinal variations in boundary layer characteristics, together with the free-surface profile and free-stream velocity, where k_s is the step cavity height: $k_s = h \times \cos\theta$. [Note the different scales for the left and right vertical axes in Fig. 4(b).] All the data showed a boundary layer thickness increasing monotonically toward the free surface, while the flow depth decreased in the downstream direction. The free-stream velocity data matched closely the solution of the Bernoulli principle, as seen in Fig. 4(b). The full data set is reported in the Appendix. The onset of free-surface aeration occurred once the boundary layer outer edge reached the close proximity of the free surface. At this point, the boundary layer thickness was about $\delta/d = \delta/d_i \approx 0.8$, and this reflected that the outer edge of the boundary layer was irregular and fluctuating (Klebanoff 1955; Antonia 1972; Phillips and Ratnanather 1990).

Compared to a smooth spillway, the steps acted as macroroughness elements, causing a more rapid boundary layer growth than on a smooth chute (Chanson 1994, 2001; Amador et al. 2009). The present data set was correlated by

$$\frac{\delta}{L} = 0.15 \times \left(\frac{L}{k_s}\right)^{-0.37} \tag{8}$$

Eq. (8) is valid for $0.9 \leq d_c/h \leq 1.7$ and $0 < L/k_s < 15$ and is compared to the data in Fig. 5. The results complemented the earlier findings of Amador et al. (2006) and Meireles et al. (2012) on 1V:0.8H and 1V:0.75H ogee-crested stepped chutes, respectively, but for larger values of L/k_s. For $L/k_s > 5$ to 10, the difference between the present data [Eq. (8)] and the data of Amador et al. (2006) and Meireles et al. (2012) tended to be small. All together, Eq. (8) was seen to provide a reasonable estimate of the boundary layer growth for all data sets (Fig. 5), suggesting that the boundary layer development was minimally influenced by the type of crest and the chute slope (namely, for $L/k_s > 10^0$).

For the entire experimental data set, the median data yielded the dimensionless ratios

$$\frac{\delta_1}{\delta} = 0.191 \tag{9}$$

$$\frac{\delta_2}{\delta} = 0.126 \tag{10}$$

$$\frac{\delta_1}{\delta_2} = 1.53 \tag{11}$$

where δ_1 = displacement thickness; δ_2 = momentum thickness; and δ_1/δ_2 = shape factor. The results [Eqs. (9)–(11)] compared well with analytical solutions for a velocity power law with an exponent

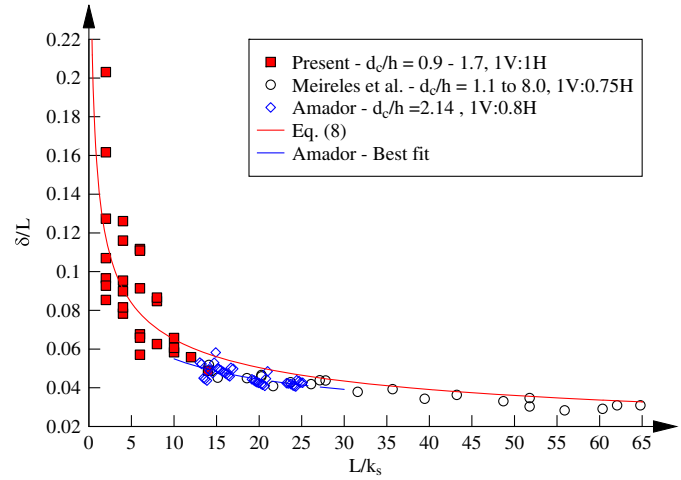

Fig. 5. Boundary layer growth in skimming flows on a stepped spillway: comparison between boundary layer thickness data [Eq. (8)] and previous experimental studies (data from Amador et al. 2006; Meireles et al. 2012)

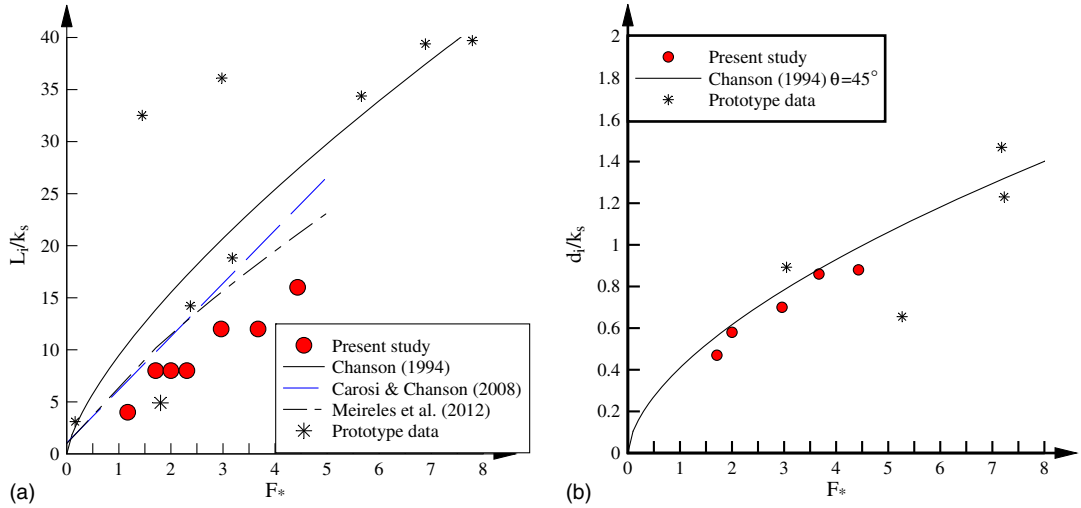

Fig. 6. Inception point of free-surface aeration in skimming flows on stepped spillways: (a) location of the inception point of free-surface aeration and comparison with prototype observations: Brushes Clough Dam (Greater Manchester, U.K.), Dona Francisca (Rio Grande do Sul, Brazil), Gold Creek Dam (Queensland, Australia), Hinze Dam (Queensland, Australia), Pedrógão (Leiria district, Portugal) (data reanalysis from Chanson et al. 2015); (b) water depth at the inception point of free-surface aeration; comparison with Eq. (13) and prototype observations at Dona Francisca (data reanalysis from Chanson et al. 2015)

$1/N = 1/4.5$ (Schlichting 1960; Chanson 2009). This value was close to observations in developing boundary layers on rough walls (Liu et al. 1966) and for the velocity distributions in the developing boundary layer at step edges (see Part II, Zhang and Chanson 2016).

Discussion: Inception Point of Free-Surface Aeration

The characteristics of the inception point of free-surface aeration were recorded for $0.7 \leq d_c/h \leq 1.7$, and the results are presented in Fig. 6. The data set is reported in Table 1. The inception point location is most commonly determined either by visual observations (Chanson 1994; Carosi and Chanson 2008; and the current study), or by void fraction measurements (Meireles et al. 2012). The former is the only means to characterize the inception point on prototype stepped spillways and enable a model-prototype comparison. The present observations showed that the inception point shifted downstream with increasing discharge. For $d_c/h > 1.9$, the entire chute flow was nonaerated. The data are plotted in Fig. 6(a), with the dimensionless length to inception L_i/k_s as a function of the dimensionless discharge F_*:

$$F_* = \frac{q}{\sqrt{g \times \sin\theta \times k_s^3}} \tag{12}$$

where $\theta = 45°$ is the chute slope. The present data were compared to prototype data and earlier empirical correlations (Chanson 1994; Carosi and Chanson 2008; Meireles et al. 2012). Fig. 6 regroups a number of prototype data, obtained for chute slopes between 18.4° and 57.4°, dimensionless discharges within $0.2 < d_c/h < 8.8$ and Reynolds numbers $2 \times 10^6 < \mathrm{R} < 7.5 \times 10^7$. The overall agreement was reasonable, although the correlations tended to overpredict the location of inception point. Herein, velocity and pressure measurements suggested that the flow was rapidly varied in the vicinity of the inception point (see Part II, in Zhang and Chanson 2016). The water depth d_i data at the inception of free-surface aeration are plotted in Fig. 6(b). The present data are compared to prototype observations and Chanson's (1994) correlation:

$$\frac{d_i}{k_s} = \frac{0.4034}{(\sin\theta)^{0.04}} \times F_*^{0.592} \tag{13}$$

The overall agreement between experimental data and correlation was good. At the inception point of air entrainment, the boundary layer outer edge was close to, but smaller than, the water depth; namely, the boundary layer thickness was about $\delta/d_i \approx 0.8$ for the entire data set. The finding was close to Wood's (1985) criterion for smooth chutes: $d_i \approx 1.2 \times \delta$. The reasoning derived from observations that the boundary layer outer edge extended to about 1.2 times the mean thickness (Daily and Harleman 1966; Schlichting 1979).

Note that both Figs. 6(a and b) are presented herein with linear scales, while the traditional literature shows such plots with log-log axes (e.g., Chanson 1994; Meireles et al. 2012), thus smoothing the data scatter in particular at very small F_*, for which the inflow conditions and flow regime might have a relatively greater influence.

Conclusion

On a stepped spillway, the steps act as macroroughness elements, contributing to enhanced turbulence. With typical design flow conditions, the water skims down the stepped chute, and the upstream flow motion is nonaerated. In the nonaerated flow region, a turbulent boundary layer develops until the outer edge of the boundary layer interacts with the free surface and air entrainment takes place: that is, downstream of the inception point of free-surface aeration. New experiments were performed in the developing flow region on a large 1V:1H stepped spillway model. The flow properties in the developing flow region were documented using a Prandtl-Pitot tube, and the results were complemented with phase-detection probe data.

The chute flow was controlled by a broad-crested weir. Critical flow conditions took place along the entire weir crest, although the pressure distributions were not hydrostatic at the upstream and

downstream ends. Downstream of the broad-crested weir, the water skimmed over the pseudobottom formed by the step edges. Upstream of the inception point, the free surface was smooth over the first few steps, although some significant free-surface curvature was observed for all discharges. The free surface became increasingly turbulent in the downstream direction. The inception point of free-surface aeration was observed when the boundary layer thickness reached 80% of the flow depth: $\delta/d_i \approx 0.8$. The characteristics of the developing boundary layer were consistent with a 1/4.5th velocity distribution power law at the step edges. The development of the boundary layer was significantly more rapid than that on a smooth chute for the same flow rate and slope, and the findings were comparable to those of previous studies. The location of the inception point and the flow depth at inception were compared successfully to previous laboratory and prototype results, as well as to Chanson's (1994) correlations.

Appendix. Developing Boundary Layer Characteristics in the Developing Flow Region

At the upstream end of the stepped chute, a boundary layer developed along the stepped invert up to the inception point of free-surface aeration, where the outer edge of the turbulent boundary layer interacted with the free surface. The basic characteristics of the developing boundary layer were derived from the measured velocity profiles. These were the boundary layer thickness δ, displacement thickness δ_1, momentum thickness δ_2 and energy thickness δ_3. Herein, the boundary thickness was defined in terms of 99% of the free-stream velocity V_o. All the data are regrouped here in a tabular format for the experimental configuration ($\theta = 45°$, $h = 0.10$ m, $W = 0.985$ m).

d_c/h	L_i (m)	d_i (m)	Step edge	x (m)	d (m)	V_o (m/s)	δ (m)	δ_1 (m)	δ_2 (m)	δ_3 (m)
0.9	0.57	0.033	2	0.14	0.048	1.98	0.0131	0.002	0.0015	0.0028
0.9	—	—	3	0.28	0.041	2.45	0.0183	0.0032	0.0018	0.0032
0.9	—	—	4	0.42	0.041	2.82	0.028	0.0053	0.0037	0.0064
1	0.57	0.041	2	0.14	0.053	2.04	0.0136	0.0025	0.0018	0.0031
1	—	—	3	0.28	0.045	2.5	0.0189	0.0035	0.0017	0.003
1	—	—	4	0.42	0.044	2.87	0.0242	0.005	0.0035	0.0059
1.1	0.57	—	2	0.14	0.06	2.09	0.0151	0.0029	0.0021	0.0036
1.1	—	—	3	0.28	0.051	2.54	0.0204	0.0039	0.0015	0.0029
1.1	—	—	4	0.42	0.05	2.9	0.0287	0.0048	0.0035	0.0062
1.3	0.85	0.049	2	0.14	0.075	2.18	0.018	0.0047	0.0027	0.0044
1.3	—	—	3	0.28	0.063	2.62	0.023	0.0036	0.0015	0.0028
1.3	—	—	4	0.42	0.058	2.98	0.0388	0.0046	0.0034	0.006
1.3	—	—	5	0.57	0.058	3.3	0.0409	0.01	0.0064	0.0108
1.5	0.85	0.061	2	0.14	0.089	2.27	0.0229	0.0101	0.0017	0.0035
1.5	—	—	3	0.28	0.075	2.7	0.0329	0.0064	0.0043	0.0074
1.5	—	—	4	0.42	0.069	3.05	0.047	0.0106	0.0068	0.0115
1.5	—	—	5	0.57	0.068	3.36	0.0515	0.0177	0.0092	0.0144
1.7	1.13	0.062	2	0.14	0.108	2.34	0.0262	0.0199	—	0.0007
1.7	—	—	3	0.28	0.089	2.77	0.0357	0.0107	0.006	0.0099
1.7	—	—	4	0.42	0.08	3.13	0.0558	0.0085	0.0062	0.0111
1.7	—	—	5	0.57	0.078	3.43	0.0479	0.0068	0.0046	0.0083

Acknowledgments

The authors thank Professor Fabian Bombardelli (University of California Davis, in the United States) and Professor Jorge Matos (IST Lisbon, Portugal) for their valuable comments. They also thank Dr. John Macintosh (Water Solutions, Brisbane, Australia) for his comments and supervisory involvement. The authors acknowledge the technical assistance provided by Jason Van de Gevel and Stewart Matthews, at the University of Queensland (Australia). The financial support of the Australian Research Council (Grant DP120100481) is acknowledged.

Notation

The following symbols are used in this paper:

C = void fraction;
C_D = dimensionless discharge coefficient: $C_D = q/(g \times (2/3 \times H_1)^3)^{1/2}$;
D_H = hydraulic diameter (m);
d = water depth (m);
d_c = critical flow depth (m);
d_i = flow depth (m) inception point of free-surface aeration;
E = specific energy (m): $E = H_t - z_o$;
$E_{\min}$ = minimum specific energy (m);
F_* = dimensionless discharge: $F_* = q/\sqrt{g \times \sin\theta \times k_s^3}$
g = gravity acceleration (m/s^2): $g = 9.80$ m/s^2 in Brisbane, Australia;
H_t = total head (m);
H_1 = upstream head above crest (m);
h = vertical step height (m);
k_s = step roughness height (m): $k_s = h \times \cos\theta$;
L = longitudinal distance (m) positive downstream measured from step edge 1;
L_{crest} = broad-crested weir length (m);
L_i = distance between step edge 1 and inception point of free-surface aeration;
M = Morton number: $\mathrm{M} = g \times \mu^4/(\rho \times \sigma^3)$;
P = pressure (Pa);
q = water discharge per unit width (m^2/s);
R = Reynolds number defined in terms of the hydraulic diameter: $\mathrm{R} = \rho \times U \times D_H/\mu$;
U = flow velocity (m/s) positive downstream;
V_c = critical flow velocity (m/s);
V_x = longitudinal velocity component (m/s);
V_o = free-stream velocity (m/s);
W = channel width (m);
x = longitudinal distance (m) positive downstream measured from step edge;
Y_{90} = characteristic distance (m) where $C = 0.90$;
y = distance (m) normal to the invert, measured perpendicular to the pseudobottom formed by the step edges (on the stepped section);
z = transverse coordinate (m);
z_o = invert elevation (m) above datum;
β = Boussinesq coefficient;
δ = boundary layer thickness (m);
δ_1 = displacement thickness (m);
δ_2 = momentum thickness (m);
δ_3 = energy thickness (m);
Λ = pressure correction coefficient;
μ = water viscosity (Pa · s);
θ = angle between pseudobottom formed by step edges and horizontal;
ρ = water density (kg/m^3);
σ = surface tension between air and water (N/m); and
Ø = diameter (m).

Subscripts

c = critical flow conditions;
i = inception point of free-surface aeration; and
90 = 90% void fraction.

References

Amador, A. (2005). "Comportamiento hidráulico de los aliviaderos escalonados en presas de hormigón compactado." Ph.D. thesis, Technical Univ. of Catalonia, (UPC), Barcelona, Spain (in Spanish).

Amador, A., Sánchez-Juny, M., and Dolz, J. (2006). "Characterization of the nonaerated flow region in a stepped spillway by PIV." *J. Fluids Eng.*, 128(6), 1266–1273.

Amador, A., Sánchez-Juny, M., and Dolz, J. (2009). "Developing flow region and pressure fluctuations on steeply sloping stepped spillways." *J. Hydraul. Eng.*, 10.1061/(ASCE)HY.1943-7900.0000118, 1092–1100.

Antonia, R. A. (1972). "Conditionally sampled measurements near outer edge of a turbulent boundary layer." *J. Fluid Mech.*, 56(1), 1–18.

Bakhmeteff, B. A. (1932). *Hydraulics of open channels*, McGraw-Hill, New York, 329.

Bombardelli, F. A., Meireles, I., and Matos, J. (2011). "Laboratory measurements and multi-block numerical simulations of the mean flow and turbulence in the non-aerated skimming flow region of steep stepped spillways." *Environ. Fluid Mech.*, 11(3), 263–288.

Carosi, G., and Chanson, H. (2008). "Turbulence characteristics in skimming flows on stepped spillways." *Can. J. Civ. Eng.*, 35(9), 865–880.

Chamani, M. R. (2000). "Air inception in skimming flow regime over stepped spillways." *Proc., Int. Workshop on Hydraulics of Stepped Spillways*, Balkema, Zürich, Switzerland, 61–67.

Chanson, H. (1994). "Hydraulics of skimming flows over stepped channels and spillways." *J. Hydraul. Res.*, 32(3), 445–460.

Chanson, H. (1995). "History of stepped channels and Spillways: A rediscovery of the 'wheel'." *Can. J. Civ. Eng.*, 22(2), 247–259.

Chanson, H. (1996). "Free-surface flows with near-critical flow conditions." *Can. J. Civ. Eng.*, 23(6), 1272–1284.

Chanson, H. (2000–2001). "Historical development of stepped cascades for the dissipation of hydraulic energy." *Trans. Newcomen Soc.*, 71(2), 295–318.

Chanson, H. (2001). *The hydraulics of stepped chutes and spillway*, Balkema, Lisse, the Netherlands, 418.

Chanson, H. (2006). "Minimum specific energy and critical flow conditions in open channels." *J. Irrig. Drain. Eng.*, 10.1061/(ASCE)0733-9437(2006)132:5(498), 498–502.

Chanson, H. (2008). "Advective diffusion of air bubbles in turbulent water flows." *Fluid mechanics of environmental interfaces*, C. Gualtieri and D. T. Mihailovic, eds., Taylor & Francis, Leiden, the Netherlands, 163–196.

Chanson, H. (2009). *Applied hydrodynamics: An introduction to ideal and real fluid flows*, CRC Press, Taylor & Francis Group, Leiden, the Netherlands, 478.

Chanson, H. (2015). "Cavitation potential of flow on stepped spillways. Discussion." *J. Hydraul. Eng.*, 10.1061/(ASCE)HY.1943-7900.0000808, 07014025.

Chanson, H., Bung, D., and Matos, J. (2015). "Stepped spillways and cascades." *Energy dissipation in hydraulic structures, IAHR monograph*, H. Chanson, ed., CRC Press, Taylor & Francis Group, Leiden, Netherlands, 45–64.

Chanson, H., and Toombes, L. (2004). "Hydraulics of stepped chutes: The transition flow." *J. Hydraul. Res.*, 42(1), 43–54.

Chanson, H., Yasuda, Y., and Ohtsu, I. (2002). "Flow resistance in skimming flows and its modelling." *Can. J. Civ. Eng.*, 29(6), 809–819.

Daily, H. W., and Harleman, D. R. F. (1966). *Fluid dynamics*, Addison-Wesley, Reading, MA, 454.

Ervine, D. A., and Falvey, H. T. (1987). "Behaviour of turbulent water jets in the atmosphere and in plunge pools." *Proc. Inst. Civ. Eng.*, 83(2), 295–314.

Felder, S., and Chanson, H. (2012). "Free-surface profiles, velocity, and pressure distributions on a broad-crested weir: A physical study." *J. Irrig. Drain. Eng.*, 10.1061/(ASCE)IR.1943-4774.0000515, 1068–1074.

Frizell, K. W., Renna, F. M., and Matos, J. (2013). "Cavitation potential of flow on stepped spillways." *J. Hydraul. Eng.*, 10.1061/(ASCE)HY.1943-7900.0000715, 630–636.

Gonzalez, C. A., and Chanson, H. (2007). "Hydraulic design of stepped spillways and downstream energy dissipators for embankment dams." *Dam Eng.*, 17(4), 223–244.

Guenther, P., Felder, S., and Chanson, H. (2013). "Flow aeration, cavity processes and energy dissipation on flat and pooled stepped spillways for embankments." *Environ. Fluid Mech.*, 13(5), 503–525.

Henderson, F. M. (1966). *Open channel flow*, MacMillan, New York, 522.

Hunt, S. L., and Kadavy, K. C. (2010). "Energy dissipation on flat-sloped stepped spillways: Part 1. Upstream of the inception point." *Trans. ASABE*, 53(1), 103–109.

Isaacs, L. T. (1981). "Effects of laminar boundary layer on a model broad-crested weir." *Research Rep. No. CE28*, Dept. of Civil Engineering, Univ. of Queensland, Brisbane, Australia, 20.

Klebanoff, P. S. (1955). "Characteristics of turbulence in a boundary layer with zero pressure gradient." *NACA Rep. No. 1247*, Boston, 20.

Liggett, J. A. (1993). "Critical depth, velocity profiles, and averaging." *J. Irrig. Drain. Eng.*, 10.1061/(ASCE)0733-9437(1993)119:2(416), 416–422.

Liu, C. K., Kline, S. J., and Johnston, J. P. (1966). "An experimental study of turbulent boundary layer on rough walls." *Rep. No. MD-15*, Dept. of Mechanical Engineering, Stanford Univ., Stanford, CA, 171.

Matos, J. (1999). "Air entrainment and energy dissipation in flow over stepped spillways (emulsionamento de ar e dissipação de energia do escoamento em descarregadores em degraus)." Ph.D. thesis, IST, Lisbon, Portugal (in Portuguese).

Meireles, I. (2004). "Characterization of the skimming flow and residual energy in stepped spillways (Caracterização do escoamento deslizante sobre turbilhões e energia específica residual em descarregadores de cheias em degraus)." M.Sc. thesis, IST, Lisbon, Portugal (in Portuguese).

Meireles, I., and Matos, J. (2009). "Skimming flow in the non-aerated region of stepped spillways over embankment dams." *J. Hydraul. Eng.*, 10.1061/(ASCE)HY.1943-7900.0000047, 685–689.

Meireles, I., Renna, F., Matos, J., and Bombardelli, F. A. (2012). "Skimming, nonaerated flow on stepped spillways over roller compacted concrete dams." *J. Hydraul. Eng.*, 10.1061/(ASCE)HY.1943-7900.0000591, 870–877.

Meireles, I. C., Bombardelli, F. A., and Matos, J. (2014). "Air entrainment onset in skimming flows on steep stepped spillways: An analysis." *J. Hydraul. Res.*, 52(3), 375–385.

Peyras, L., Royet, P., and Degoutte, G. (1992). "Flow and energy dissipation over stepped gabion weirs." *J. Hydraul. Eng.*, 10.1061/(ASCE)0733-9429(1992)118:5(707), 707–717.

Phillips, W. R. C., and Ratnanather, J. T. (1990). "The outer region of a turbulent boundary layer." *Phys. Fluids A-Fluid Dyn.*, 2(3), 427–434.

Rajaratnam, N. (1990). "Skimming flow in stepped spillways." *J. Hydraul. Eng.*, 10.1061/(ASCE)0733-9429(1990)116:4(587), 587–591.

Rao, N. S. G., and Rajaratnam, N. (1961). "On the inception of air entrainment in open channel flows." *Proc., 9th IAHR Biennial Congress*, IAHR, 9–12.

Renna, F. (2004). "Phenomenological characterization of two-phase flow along stepped spillways (Caratterizzazione fenomenologica del moto di un fluido bifasico lungo scaricatori a gradini)." Ph.D. thesis, Politecnico di Bari, Cosenza, Italy (in Italian).

Schlichting, H. (1960). *Boundary layer theory*, 4th Ed., McGraw-Hill, New York.

Schlichting, H. (1979). *Boundary layer theory*, 7th Ed., McGraw-Hill, New York.

Wood, I. R. (1985). "Air water flows." *Proc., 21st IAHR Biennial Congress*, IAHR, 18–29.

Wood, I. R., Ackers, P., and Loveless, J. (1983). "General method for critical point on spillways." *J. Hydraul. Eng.*, 10.1061/(ASCE)0733-9429(1983)109:2(308), 308–312.

Zhang, G., and Chanson, H. (2015). "Hydraulics of the developing flow region of stepped cascades: An experimental investigation." *Hydraulic Model Rep. No. CH97/15*, School of Civil Engineering, Univ. of Queensland, Brisbane, Australia, 76.

Zhang, G., and Chanson, H. (2016). "Hydraulics of the developing flow region of stepped spillways. II. Pressure and velocity fields." *J. Hydraul. Eng.*, 04016016.